Orogenic Convection in Subtropical South America as Seen by the TRMM Satellite

KRISTEN L. RASMUSSEN AND ROBERT A. HOUZE JR.

Department of Atmospheric Sciences, University of Washington, Seattle, Washington

(Manuscript received 7 October 2010, in final form 25 February 2011)

ABSTRACT

Extreme orogenic convective storms in southeastern South America are divided into three categories: storms with deep convective cores, storms with wide convective cores, and storms containing broad stratiform regions. Data from the Tropical Rainfall Measuring Mission satellite's Precipitation Radar show that storms with wide convective cores are the most frequent, tending to originate near the Sierra de Cordoba range. Downslope flow at upper levels caps a nocturnally enhanced low-level jet, thus preventing convection from breaking out until the jet hits a steep slope of terrain, such as the Sierra de Cordoba Mountains or Andean foothills, so that the moist low-level air is lifted enough to release the instability and overcome the cap. This capping and triggering is similar to the way intense convection is released near the northwestern Himalayas. However, the intense storms with wide convective cores over southeastern South America are unlike their Himalayan counterparts in that they exhibit leading-line/trailing-stratiform organization and are influenced by baroclinic troughs more similar to storms east of the Rocky Mountains in the United States. Comparison of South American storms containing wide convective cores with storms in other parts of the world contributes to a global understanding of how major mountain ranges influence precipitating cloud systems.

1. Introduction

Observations from the Tropical Rainfall Measuring Mission (TRMM) satellite have led to the realization that intense storms just east of the Andes in southeastern South America are among the most intense anywhere in the world (Zipser et al. 2006). The other ''hot spots'' of extreme deep convection are over the plains east of the Rocky Mountains in the United States and near the western Himalayas in South Asia. All three hot spots occur near a major mountain range that is indicative of the orogenic[1] nature of storms in these locations. Supercell thunderstorm formation and mesoscale storm structure over the Great Plains of the United States have been extensively studied. For example, Carlson et al. (1983) documented the conditions associated with supercell development, and Houze et al. (1990) showed the tendency for storms over the Great Plains to develop into mesoscale convective systems with leading lines of intense convection and trailing-stratiform precipitation. Both the central United States and southeastern South America, moreover, have large numbers of mesoscale systems satisfying Maddox's (1980) criteria to be classified as ''mesoscale convective complexes (MCCs).'' On average, South American MCC cloud shields are 60% larger than those over the United States (Velasco and Fritsch 1987), the convection is deeper (Zipser et al. 2006), and they have larger precipitation areas than those over the United States or Africa (Durkee et al. 2009). Cecil (2009, 2011) has used TRMM Microwave Imager (TMI) data to objectively identify hailstorms and found southeastern South America to be a likely region of large hail production. Extreme convective storms over southeastern South America are also associated with a large number of fatalities, flooding events, hailstorms, and tornadoes (Altinger de Schwarzkopf and Russo 1982; Nascimento and Marcelino 2005). Thus, southeastern South America is an important natural laboratory and socioeconomic venue for studying the climatological factors controlling severe weather near a major mountain range.

Over the U.S. Great Plains region, a moist low-level flow originating from the Gulf of Mexico is typically ''capped'' by drier air flowing off the Mexican Plateau

[1] Originally defined in Tripoli and Cotton (1989) as ''genesis under orographic influences.''

Corresponding author address: Kristen Lani Rasmussen, Dept. of Atmospheric Sciences, University of Washington, Box 351640, Seattle, WA 98195.
E-mail: kristen@atmos.washington.edu

DOI: 10.1175/MWR-D-10-05006.1

and the Rocky Mountains. This capping inversion inhibits the release of instability over large areas, while enhancing the intensity of convective outbreaks in narrowly focused regions (Carlson et al. 1983). Similar low-level moist flows capped by drier air coming across a major terrain feature characterize convection upstream of the western Himalayas (Houze et al. 2007). The severe convection in the U.S. and Himalayan regions, however, is released differently. The western Himalayan convection is released by flow over topography (Medina et al. 2010), whereas other features such as frontal or dryline convergence are the primary triggering mechanisms in the United States. Garreaud and Wallace (1998) and Romatschke and Houze (2010) have shown that, during the summer season in southeastern South America, frequent passages of baroclinic troughs and frontal systems over the Andes are associated with deep convection east of the mountain range. Velasco and Fritsch (1987), Zipser et al. (2006), and others have further pointed out that a topographically guided low-level jet bringing moist air poleward affects the occurrence of intense convection east of the Andes in South America in a manner similar to processes east of the Rocky Mountains in the United States. In the western Himalayan region, it is the low-level flow streaming onshore from the Arabian Sea through the gap between the Western Ghats to the south and Himalayan and Afghan mountains to the north that feeds the severe convection (Sawyer 1947; Houze et al. 2007).

Identifying common features and differences between the mechanisms producing extreme convection near the different major mountain ranges of the world will be an essential step toward a general understanding of orographic precipitation on a global scale. In this paper, we focus on the region near the Andes to better understand its similarities to and differences from orographically influenced convection in other parts of the world. We use the methodology developed by Houze et al. (2007), Romatschke et al. (2010), and Romatschke and Houze (2010) to characterize the TRMM Precipitation Radar (PR) data in regions of extreme convection. Their technique capitalizes on the TRMM PR's ability to observe fine details of the vertical and horizontal structures of radar echoes. They determine which storms have radar echoes with exceptionally intense convective cores and which storms contain extremely broad stratiform precipitation regions. Separating South American extreme storms into these categories and determining the preferred times and locations of each type will provide a basis for comparison to the structure, organization, and behavior of extreme storms in the other regions of the world observed by the TRMM satellite. The following specific questions are addressed by the present study:

- What are the most common types of extreme storm structure in South America?
- Where do these storm structures preferentially occur?
- What are the vertical and horizontal size distributions of the storm structures?
- How does storm evolution affect the geographical distribution of storm types?
- What is the preferred mesoscale organization of the major storm types?
- How do they compare with precipitating convective systems near other major mountain ranges?

In answering the first three questions, we build on the work of Romatschke and Houze (2010). They provided a climatological mapping of the storm types over the whole continent. We further examine this mapping to determine the relative importance of the different categories of storm types that they identified. We will show that the most frequent type of storm contains cores of intense convection that tend to be organized in lines with trailing-stratiform precipitation, and that these storms are most common in the La Plata Basin of Argentina and surrounding areas—the exact region singled out in Zipser et al. (2006) as having some of the most intense convection in the world. We further show that these storms are primarily responsible for the severe weather events (hail, tornadoes, and floods) in this region.

The work of Romatschke and Houze (2010) suggested that the climatological pattern of occurrence of the storm types that they identified might be explained by mesoscale storm evolution wherein storms form as more isolated deep convective cells at the edge of the Andes, move eastward and grow into mesoscale systems, and ultimately develop broad stratiform precipitation regions far to the east of the mountains. However, since they were analyzing the snapshots of data provided by TRMM, they could not verify this hypothesis. In this study, we include geosynchronous satellite data to better understand how mesoscale systems in the La Plata Basin region evolve. We examine two representative case studies with the geosynchronous data, synoptic observations, and other information to elucidate the fundamental mechanisms responsible for the formation, growth, and propagation of severe convection in southeastern South America and to compare it with storms in other parts of the world. This work will lay the groundwork for a high-resolution mesoscale modeling study of storms in this region in a future study.

2. Data and methods of analysis

This study uses 11 yr (1998–2008) of version 6 data from the TRMM Precipitation Radar (PR) during the

TABLE 1. Number of storm reports by storm category, collected from local media sources in South America. Any fatalities, hail reports, tornado reports, flood reports, power outages, and people wounded from storm-related events were counted. For the heavy/record rain category, rain rates exceeded 7.6 mm h^{-1} or total accumulation exceeded 1 m during the storm. Strong wind reports were based on the Beaufort scale from categories 9 to 12 (wind speed >20 m s^{-1}). The number of people evacuated due to a storm had to exceed 200 people to be included as a storm report.

	Fatalities	Hail	Tornado	Flood	Heavy/ record rain	Power outage	Strong wind	Evacuated	Crop damage	Injured	Total storm reports	Total No. of people affected
Deep convection	23	29	14	67	69	37	50	64 931	19	99	285	65 053
Wide convection	27	41	9	49	71	32	62	17 705	12	135	276	17 867
Broad stratiform	43	24	5	31	44	18	37	15 096	20	65	179	15 204

austral spring through fall months (September–April). The following data products are used:

- 2A23—rain characteristics (Awaka et al. 1997), which classifies rain into three categories: convective, stratiform, and other; all references to convective and stratiform precipitation in this paper are based on these classifications; and
- 2A25—rainfall rate and profile (Iguchi et al. 2000a,b), which provides the attenuation-corrected three-dimensional reflectivity data.

From these resources, we compile a database of the most intense storms in the three storm categories used by Houze et al. (2007), Romatschke et al. (2010), and Romatschke and Houze (2010). Following these studies, we identify those contiguous three-dimensional echo structures that have 1) deep convective cores (40-dBZ echo $\geq$10 km in maximum height), which are associated with severe weather and vigorous convection; 2) wide convective cores (40-dBZ echo $\geq$1000 km^2 when projected onto a horizontal plane), which are normally associated with mesoscale convective systems (MCSs) in a fairly early stage; and 3) broad stratiform regions (stratiform echo $\geq$50 000 km^2 when projected onto a horizontal plane), which are normally associated with later-stage MCSs. These properties identify the most extreme vertical and horizontal structures exhibited by the PR echoes.

To identify storms with these properties, we follow data-processing procedures described by Houze et al. (2007). The PR data are remapped and interpolated into Cartesian coordinates, with a vertical resolution of 0.25 km. From the Cartesian data, we identify the top 50 storms, by height or area, in each category and compile a set of three-dimensional analyses detailing their structures. Horizontal and vertical cross sections of each case are then examined to gain insights into the structures of the convective cells and stratiform regions of the most intense storms. Automated procedures are used to determine the characteristics of echoes satisfying the three extreme-structure categories. Geostationary Operational Environmental Satellite (GOES) data, Twentieth Century reanalysis data (Compo et al. 2009), and National Centers for Environmental Prediction–National Center for Atmospheric Research (NCEP–NCAR) reanalysis data (Kalnay et al. 1996) are examined to determine the larger-scale context of the extreme storms.

We further categorize the three extreme types of radar echo structures by their mesoscale organization in a method similar to that of Houze et al. (1990) and Schiesser et al. (1995). These previous studies applied this methodology to storms producing major rainfall in Oklahoma (Houze et al. 1990) and hailstorms in Switzerland (Schiesser et al. 1995) to determine the degree to which the radar echoes in storms consisted of leading convective lines and trailing-stratiform regions. Additionally, local media sources in southeastern South America contribute to the storm analysis by corroborating extreme storm impacts. A summary of these severe storm reports by storm category is shown in Table 1. Our study of the same properties of South American storms facilitates comparisons to storms over the central United States and other regions.

3. Climatology of storms containing deep convective cores, wide convective cores, and broad stratiform regions

To obtain an overview of the occurrence of the three categories of radar echo structure defined in section 2, we broadly examine their interannual, seasonal, and regional variabilities. The regions we focus on in this study are indicated in Fig. 1. The deepest and most horizontally extensive intense convective echoes occur in the areas called the Sierra de Cordoba (see inset in Fig. 1) and La Plata Basin South. Atmospheric moisture

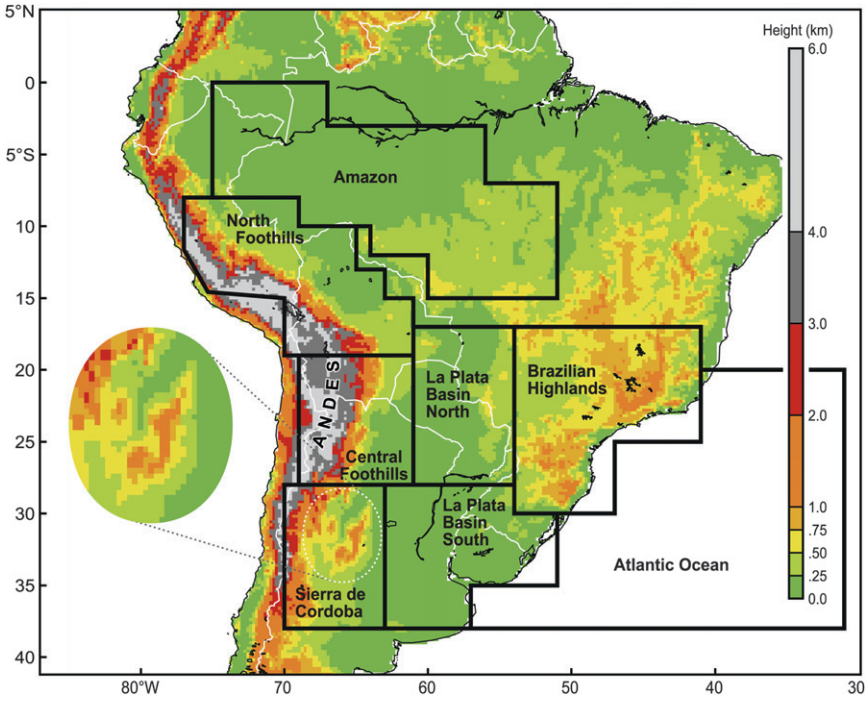

FIG. 1. Topographical map of South America showing the Andes mountain range and associated terrain features. Selected regions for this study are outlined in black and labeled. Circular inset highlights the Sierra de Cordoba range that is of particular importance to this study.

located over the Amazon basin generally flows southward in a narrow zone just east of the Andes through the regions denoted as the North Foothills and Central Foothills and is commonly referred to as the South American low-level jet (SALLJ; Nogués-Paegle and Mo 1997; Vera et al. 2006; Saulo et al. 2000, and others). Convection forming and growing in these regions typically moves eastward toward the Brazilian Highlands and the Atlantic Ocean. Romatschke and Houze (2010) found that deep convective cores tend to be triggered at about 30°–35°S in the Andean foothills and in the Sierra de Cordoba range, a smaller, north–south-oriented mountain chain just east of the Andes (Fig. 1, inset).

a. Overall statistics of extreme radar echo structures

The relative percentage of storms that occur per storm category each year in all of the regions combined is shown in Fig. 2. The wide convective category is the most frequent throughout the year on average. Assuming that the TRMM PR seldom resamples the same storm, this statistic shows that storms with wide convective cores do not necessarily evolve from storms with deep convective cores, nor do they always evolve into storms with broad stratiform regions.

Individual instances of storms containing deep convective cores, wide convective cores, or broad stratiform regions are usually embedded in a larger contiguous echo region. These contiguous echoes typically contain a mix of convective and stratiform precipitation. Figure 3a shows the volume of rain falling from larger echoes containing deep convective cores, wide convective cores, and broad stratiform regions. Most of the storms containing the 50 deepest convective cores had a very high convective rain percentage (80%–100%) and relatively low volumetric rain rate. In contrast, storms with broad stratiform regions had low convective rain percentages (0%–40%) and substantially higher volumetric rain rates. The storms with wide convective cores span the two other categories in convective rain percentage with a range of 40%–100%, but their volumetric rain rates were similar to the broad stratiform areas. These statistics indicate that the separation of storms according to whether they contain these three categories of extreme echo structures effectively characterizes storm variations by both precipitation type and amount.

Figure 3b compares the volumetric rain rate to the number of lightning flashes, which is derived from the Lightning Imaging Sensor (LIS) aboard the TRMM satellite. Consistent with Fig. 3a, most of the storms with broad stratiform regions have little to no lightning. The storms containing deep convective cores show a large range in the number of lightning strikes, from 20 to over

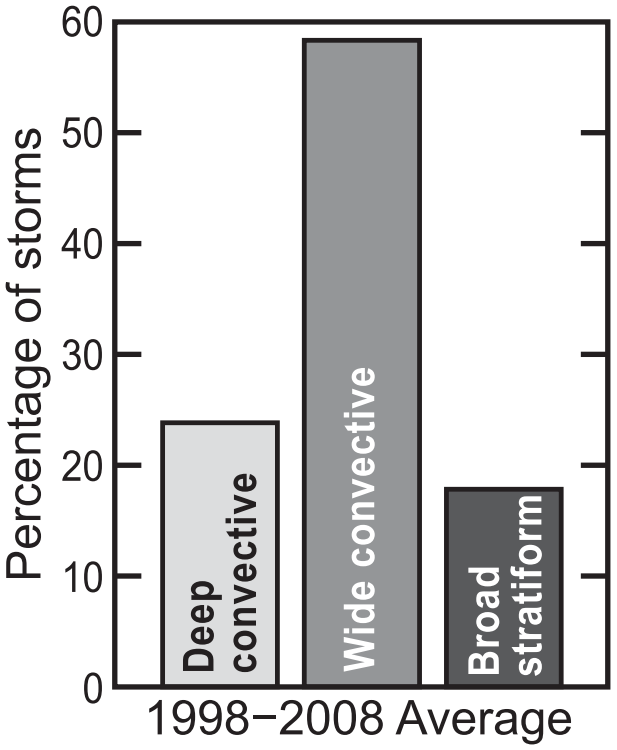

FIG. 2. Bar graph showing the average percentage of storms that occur in each storm category in all regions combined. Averages were taken from 11 yr of data (1998–2008).

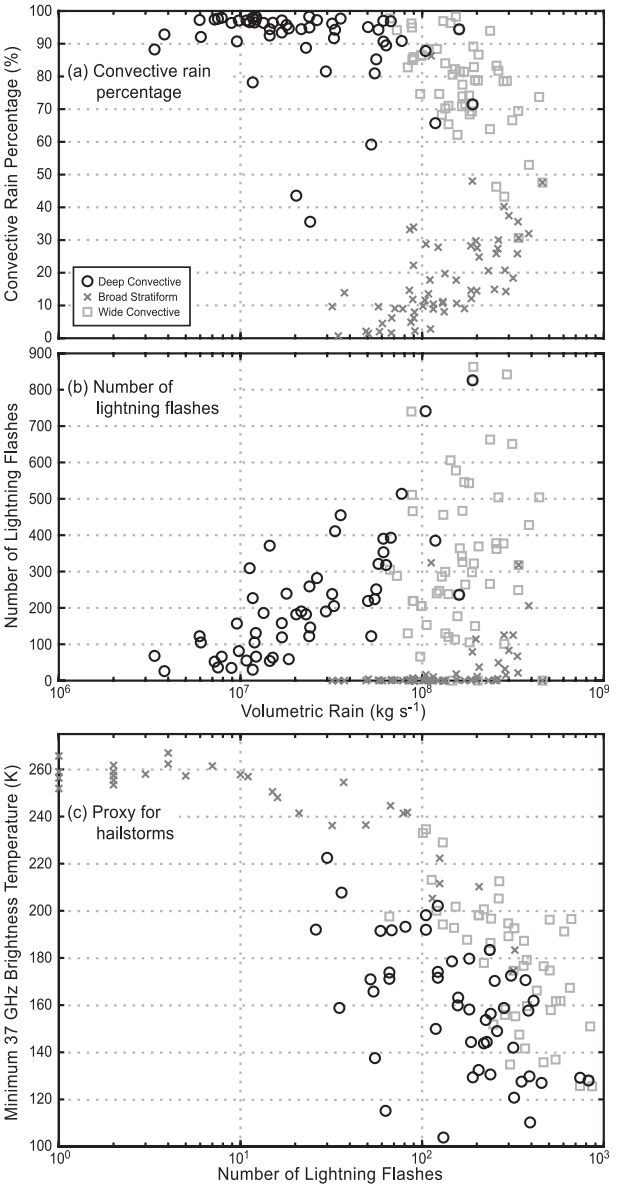

FIG. 3. (a) Scatterplot of convective rain percentage (%) and volumetric rain rate (kg s^{-1}) for the three storm categories. Deep convective cores are represented by circles (○), wide convective cores are squares (□), and broad stratiform regions by × marks. (b) Scatterplot of the number of lightning flashes observed by the LIS aboard the TRMM satellite and volumetric rain rate (kg s^{-1}). (c) Scatterplot of the minimum 37-GHz brightness temperatures (K) from the TMI and number of lightning flashes as a proxy for hailstorms as defined in Cecil (2009). Symbols are the same for all panels. All values are derived from TRMM PR, LIS, and TMI data and algorithms. Note the values on the abscissa are log scale.

700. Overall, storms containing wide convective cores have more lightning flashes than those containing deep convective cores, probably because they cover more area. In an effort to validate hailstorms around the world, Cecil (2009, 2011) found that the minimum 37-GHz microwave radiometer brightness temperatures below 180 K form an excellent proxy for hailstorms. Figure 3c compares the number of lightning flashes to the hailstorm proxy defined by Cecil (2009, 2011). The lightning data separate distinctly among the three types of storms. Only one storm with a broad stratiform region has a brightness temperature below the threshold, but there are many storms with deep and wide convective cores that fit this criterion and thus most likely contain large hail, with the wide convective cores (probably because of their greater area coverage) generally having the most flashes. According to Cecil (2009), 60% of storms with at least 125 lightning flashes per minute have hail reports, and many of the storms with deep and wide convective cores fit into this category as well.

Figure 4 compares composite hodographs that were extracted from the NCEP–NCAR reanalysis data from the inflow region of the storms with the 50 most intense deep and wide convective cores. Proximity soundings extracted from the NCEP–NCAR reanalysis dataset were used by Brooks et al. (2003) to identify regions around the world that are favorable for severe or tornadic thunderstorms. Southeastern South America was identified as a very favorable region for both severe and

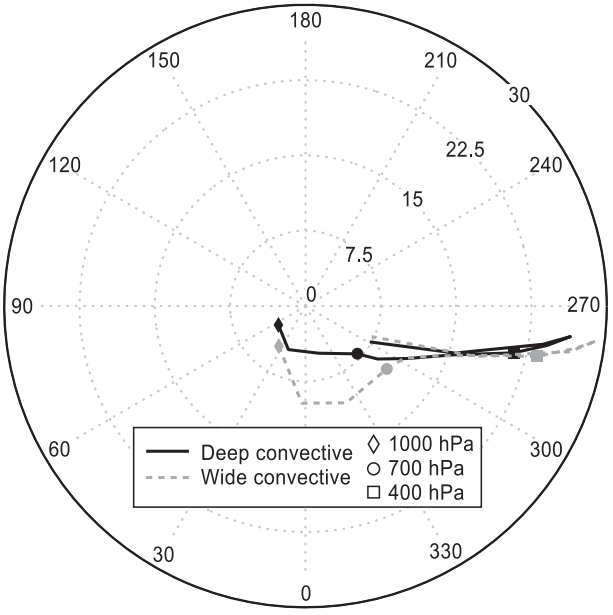

FIG. 4. Composite hodographs for the 50 storms with the most intense deep and wide convective cores. Individual wind profiles were extracted from NCEP–NCAR reanalysis data in the inflow region of each storm before compositing. Numbers outside the largest circle are meteorological wind directions and dotted rings in the interior indicate wind speeds (m s^{-1}). Vertical profiles of wind direction and speed are for storms with deep convective cores (solid) and wide convective cores (dashed). Diamond symbols indicate the 1000-hPa level, circle symbols indicate 700 hPa, and square symbols indicate the 400-hPa level.

tornadic thunderstorms based on various thermodynamic and wind shear criteria. While the usefulness of this technique was demonstrated by Brooks et al. (2003), they also mention that magnitudes of the low-level wind shear are generally less than are seen in rawinsonde data, consistent with the idea that ''strong vertical gradients are not reproduced well in the reanalysis.'' For the current study, Fig. 4 shows that the vertical profile of the environmental horizontal wind vector for storms with wide convective cores (dotted line) exhibits a much stronger low-level jet signature, producing a counterclockwise turning of the shear with height. In the United States, this type of curved hodograph has been associated with supercell storms, which produce both tornadoes and hail (Maddox 1976). The curved hodograph in Fig. 4 is consistent with the storms with wide convective cores in southeastern South America being supercellular, with attendant tornadoes and/or large hail, as has been found to be the case by Altinger de Schwarzkopf and Russo (1982) and Nascimento and Marcelino (2005). We will show in section 6 that tornadoes and hail are indeed associated with the storms classified as wide convective cores. In contrast, the deep convective cores are associated with a straight hodograph.

b. Seasonal and regional variabilities of extreme radar echo structures

A seasonal summary of all three storm categories by geographic region is shown in Fig. 5. Figure 5a shows the number of deep convective cores for all eight regions separated by month. The Sierra de Cordoba and Central Foothills regions have different overall numbers, but their seasonal cycles have a similar peak around December–January. This peak occurs during the austral summer season in which the southernmost extent of warm and moist air reaches the Sierra de Cordoba region, as will be shown in section 4. Both regions are located along the foothills of the Andes, implying a tendency for deep convective cores to be triggered along the lower foothills of the topography, as has been found in the Himalayan region (Houze et al. 2007; Medina et al. 2010). A contrasting seasonal cycle occurs in the Amazon and Atlantic regions, where a minimum occurs during December and January with few or zero deep convective cores. The Brazilian Highlands and La Plata North and South regions show a general increase during the spring, summer, and fall, with October being a particularly active month for all three.

The statistics for storms exhibiting wide convective cores (Fig. 5b) are similar to those for storms with deep convective cores (Fig. 5a) in the Sierra de Cordoba and Central Foothills regions. The Sierra de Cordoba region has higher overall numbers with a similar seasonal pattern to the Central Foothills region. The La Plata South region follows a similar seasonal cycle as these two regions with a strong increase in October. However, the Amazon and Atlantic region frequencies are strikingly different from those in Fig. 5a, exhibiting not a minimum but instead a significant number of events in the summer. The Amazon region shows a strong preference for the spring and early summer seasons and the Atlantic region shows a strong preference for the late summer and fall seasons. The statistics of storms with wide convective cores in the Brazilian Highlands, La Plata North, and North Foothills regions (Fig. 5b) mirror those of storms with deep convective cores (Fig. 5a), where both exhibit large numbers of events and decrease gradually throughout the three seasons.

Figure 5c shows the Atlantic region as the most prevalent location for storm systems with broad stratiform areas, containing almost twice as many cases as any other region. Unlike Fig. 5b, the peak values occur at the beginning of spring and then a gradual decrease occurs through autumn. The Amazon region has more broad stratiform cases during the summer and fall seasons,

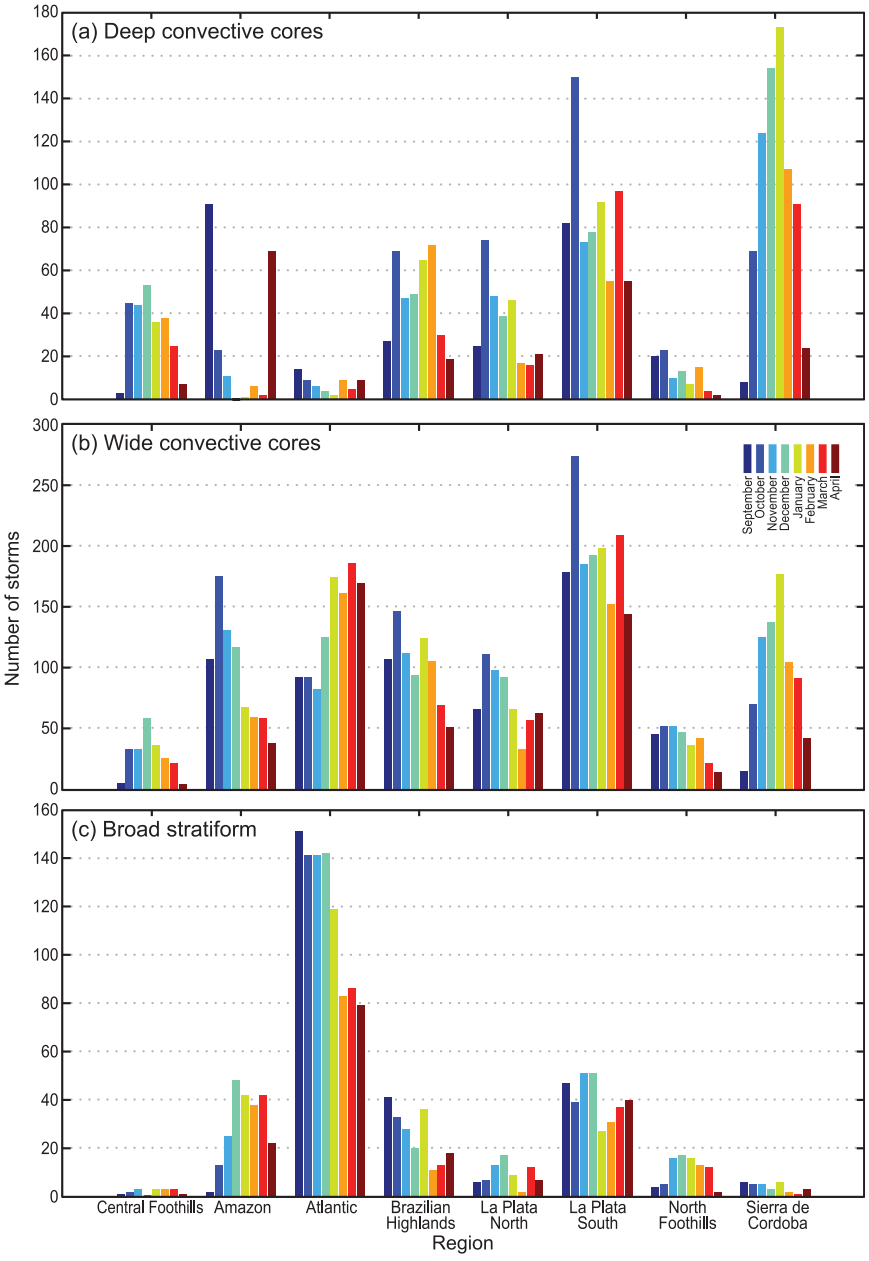

FIG. 5. (a) Number of storms with deep convective cores seen by the TRMM PR in each region outlined in Fig. 1, separated by month. Each month is represented with a different color, shown in the legend in (b). (b),(c) As in (a), but for storms with wide convective cores and storms containing broad stratiform regions, respectively. Note the values on the ordinate are different for (a)–(c).

which is a different distribution than that for the wide convective cores. The seasonal cycle in the North Foothills and La Plata North regions is similar to that of the Amazon basin. The Brazilian Highlands and La Plata South regions show a slight decrease in the spring seasons with an increase in the late summer through the fall seasons. The Sierra de Cordoba and Central Foothills regions have very few broad stratiform areas throughout all three seasons. Comparisons between regional distributions of the three storm categories are consistent with the idea that the storms tend to trigger near the foothills of the Andes, propagate eastward, and then grow to form storms with both wide convective cores and (later) broad stratiform areas.

Figure 6 shows the size distribution of storms with deep convective cores, wide convective cores, and broad stratiform regions by geographical region. For storms containing deep convective cores (Fig. 6a), the regions with the most intense events (highest extent of the 40-dBZ echo) are the Sierra de Cordoba and La Plata South regions. This result is consistent with those of Zipser et al. (2006), which indicates this exact region as the location of some of the deepest convection in the world. The Central Foothills region has a substantial number of storms containing deep convective cores, but they are not as numerous as in the regions to the south. A possible explanation for this difference is the triggering of deep convective cells by the Sierra de Cordoba range or more frequent baroclinic zones due to frontal passages in subtropical South America (Nogués-Paegle and Mo 1997; Garreaud and Wallace 1998; Liebmann et al. 1999).

The regions consistently containing the most frequent wide convective cores in any size category are the La Plata North and La Plata South regions, especially the southern choice (Fig. 6b). These two regions are east of the Andes and their relative abundance of storms with wide convective cores supports the hypothesis that echo regions containing convective cores expand as they propagate to the east. However, there are also numerous wide convective cores occurring in the Sierra de Cordoba region, which could indicate that echoes expand horizontally before moving out of this region or without propagating eastward at all in some situations.

For the broad stratiform category (Fig. 6c), the regions with the most extreme events (largest horizontal extent of contiguous stratiform pixels) are the Atlantic and La Plata South regions. As pointed out by Romatschke and Houze (2010, their Fig. 5), this regional distribution is also consistent with systems beginning as more isolated storms with deep convective cores, then propagating eastward while growing into storms containing wide convective cores. Even later, the storms develop broad stratiform areas by the time they reach their most eastward destinations. The Brazilian Highland region has fewer intense stratiform areas but is also consistent with this idea.

4. Synoptic climatology of extreme radar echo structures

From the climatology in section 3, storms with wide convective cores stand out as being significant. They are the most frequent type of extreme convection (Fig. 2), and they are associated with large volumetric rainfall, which is contributed by a combination of convective and stratiform components (Fig. 3). According to Fig. 4, storms with wide convective cores have a strong counterclockwise wind shear rotation with height, which has been associated with tornadic supercells in other regions of the world (Maddox 1976). The data in Figs. 5 and 6 further show that the storms with wide convective cores are most frequent and largest over the Sierra de Cordoba and La Plata Basin North and South regions. These facts led us to focus the remainder of this paper on storms with wide convective cores in the Sierra de Cordoba and La Plata South and North regions.

Figure 7a shows a composite sea level pressure and wind climatology computed from the Twentieth Century reanalysis data from 11 yr (1998–2008), on days when the TRMM PR showed storms containing wide convective cores over the Sierra de Cordoba and La Plata South and North regions. Persistent high pressure systems dominate over the Pacific and Atlantic Oceans (Fig. 7a). The Andes mountain range clearly affects the surface wind field by deflecting westerly winds to the north as part of the high pressure system over the Pacific. Over the continent, there is a general low pressure area on the lee side of the Andes mountain range, which is frequently referred to as the northwest Argentina low, often generated as a lee trough by approaching synoptic systems (Seluchi et al. 2003b). Ahead of these approaching baroclinic waves, warm air from the Amazon basin is channeled southward along the Andes Mountains by the northerly component winds of the SALLJ (Saulo et al. 2000; Vera et al. 2006; Marengo et al. 2004; Nogués-Paegle and Mo 1997). Previous studies have implicated the SALLJ in the occurrence of convection in southeastern South America (Salio et al. 2007; Anabor et al. 2008; Borque et al. 2010; Romatschke and Houze 2010). The seasonal progression of precipitable water and temperature, composited from days containing storms with wide convective cores, is presented in Figs. 7b and 7c. These figures show the influence of the SALLJ in bringing moist, warm air from the Amazon region into the higher latitudes in situations supporting storms with wide convective cores in southeastern South America during the austral spring–fall seasons.

As mentioned earlier, previous studies have hypothesized that the synoptic setting for storms in southeastern South America bears a resemblance to storms over the Great Plains of the United States (Carlson et al. 1983; Velasco and Fritsch 1987). In the United States, dry subsiding air from the large elevated desert region of the Mexican Plateau forms a capping inversion over moist air from the Gulf of Mexico. The capping inversion holds back the release of instability until the cap is broken by lifting, usually along a front or ahead of a midlevel trough. Smaller-scale topographic features over the plains states sometimes trigger strong convective

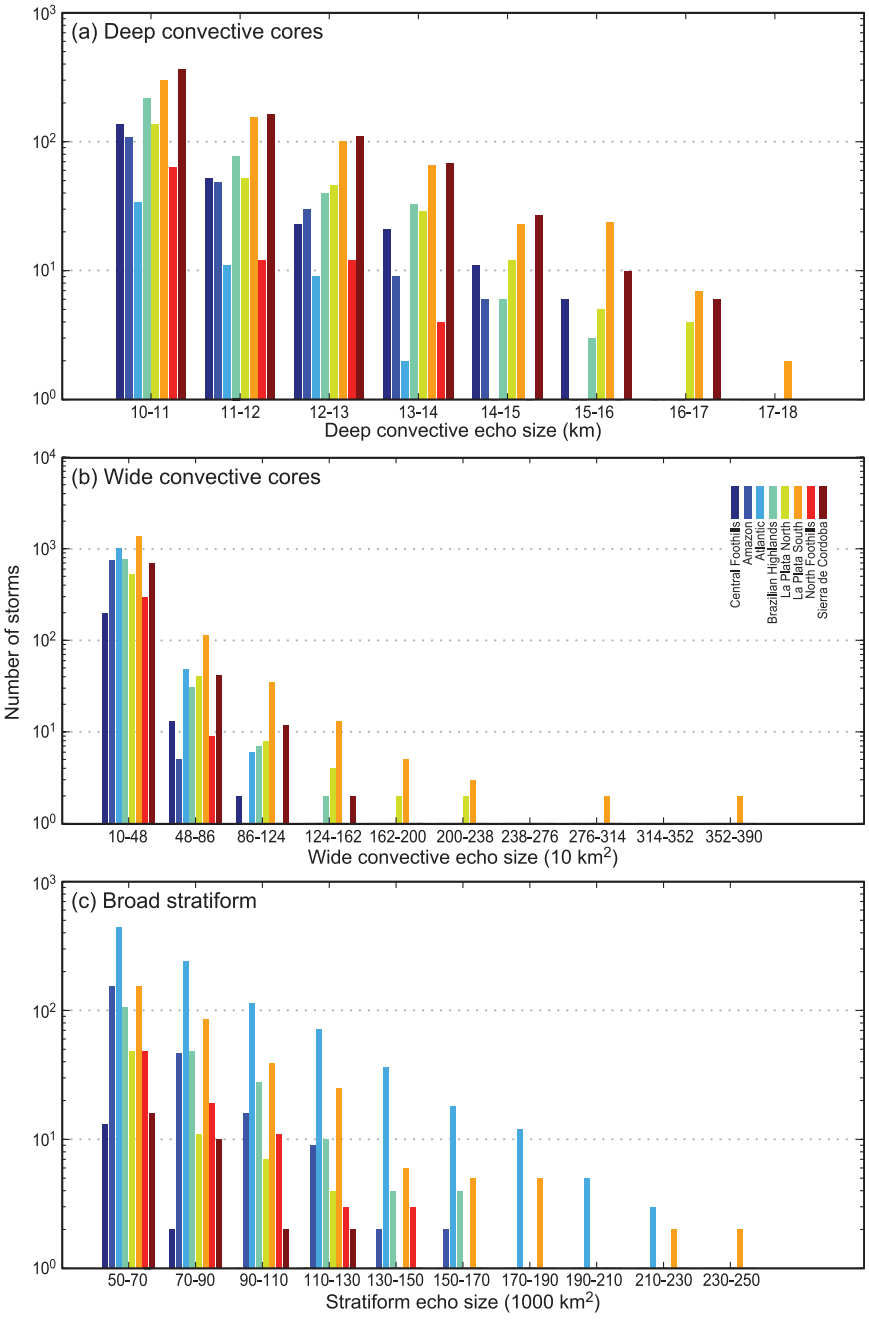

FIG. 6. (a) Vertical height of the 40-dBZ echo for storms with deep convective cores separated by region. Each region is represented with a different color. The most intense deep convective cores are characterized by having the highest extent of the 40-dBZ echo. (b) Horizontal extent of the contiguous 40-dBZ echo for storms with wide convective cores separated by region. The most intense wide convective cores have the largest extent of the 40-dBZ echo. (c) Horizontal extent of contiguous stratiform pixels, as identified by the TRMM 2A23 algorithm, for storms containing broad stratiform regions divided by region. The largest broad stratiform regions have the greatest extent of stratiform pixels. All classifications and measurements are derived from TRMM PR data. Note the values on the ordinate are log scale and different for (a)–(c).

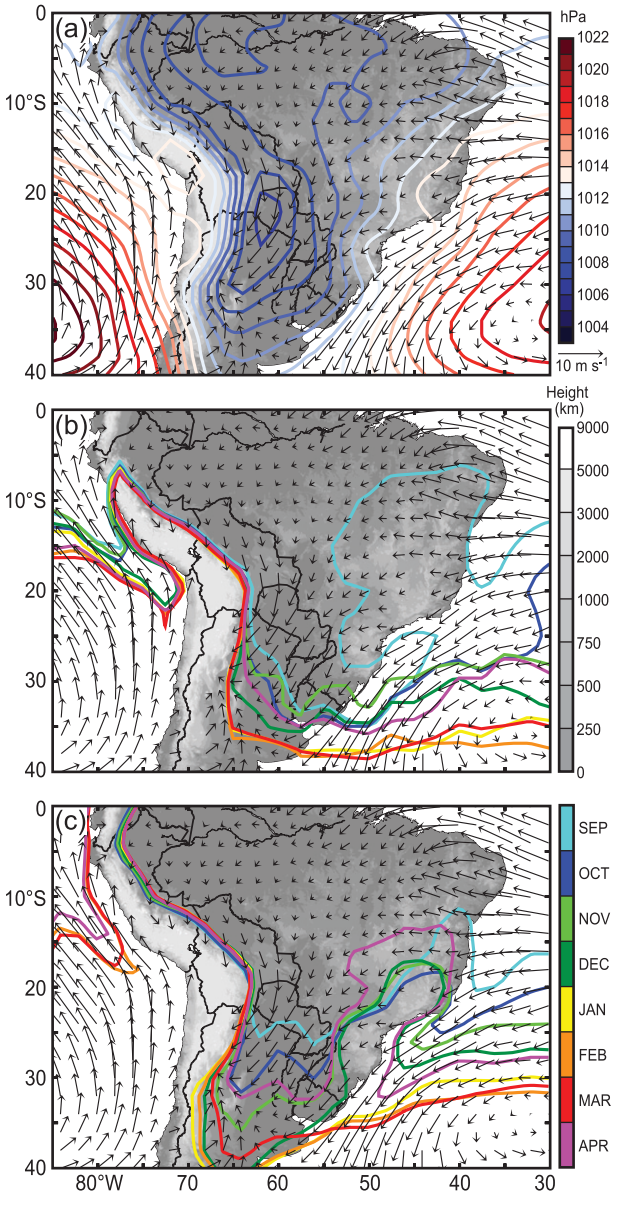

FIG. 7. Climatological composite maps for days on which the TRMM PR showed storms containing wide convective cores over the Sierra de Cordoba and La Plata North and South regions. (a) Sea level pressure (hPa) climatology composite for South America. Wind vectors at 1000 hPa were composited for the same time period and show a strong SALLJ and easterly flow into the Amazon basin. (b) Composite of the monthly progression of precipitable water (28-mm contour) in South America. Each month is represented by a color contour and the color scale is located on the eastern ordinate of (c). (c) Composite of the monthly progression of near-surface air temperature (23°C contour). Each month is represented by a color contour and the scale is the same as in (b). The topographic scale for (a)–(c) is located on the ordinate of (b). Climatology data are from the Twentieth-Century Reanalysis Dataset (Compo et al. 2009) and are used for higher-resolution maps over South America.

events. An example is the Cap Rock escarpment in northwest Texas (Smull and Houze 1985). However, these features do not dominate the statistics of extreme convective events as strongly as do the Sierra de Cordoba range and surrounding Andean foothills in southeastern South America (Romatschke and Houze 2010).

In South America, moist air from the Amazon is also capped, but for a different reason. The vertical motion composite climatology at 700 hPa for days on which storms with wide convective cores were identified in the Sierra de Cordoba and La Plata Basin regions is presented in Fig. 8a. In subtropical South America (from 20° to 40°S), mean upward motion occurs on the windward side of the Andes mountain range and is coupled with downward motion on the leeward side. This vertical motion signature is a nondiurnal effect clearly associated with the mean westerlies crossing the Andes at these latitudes. The mean values of the downward motion are not very large, but they are evidently sufficient to cap the convection just east of the Andes. Borque et al. (2010) examined a high-resolution model case study and noted that preceding the outbreak of a large MCS, the genesis region (near the Sierra de Cordoba range) experienced midlevel drying resulting from subsidence preceding the passage of an upper-level trough over the Andes Mountains (see their Figs. 7 and 14). Their results thus corroborate the pattern in our Fig. 8.

For intense convection to break out in the Sierra de Cordoba region, it must be triggered by low-level convergence sufficient to break through the cap. The 1000-hPa composite wind pattern for the same days is shown in Fig. 8b. The SALLJ is strongly evident and flows underneath the downslope subsidence. The convergence that occurs as the SALLJ encounters the Sierra de Cordoba range is in the location where Romatschke and Houze (2010) showed that intense deep convective cores prefer to form. They also showed that convective triggering is partly synoptic, as it is also favored by the presence of a trough. In the case of the Himalayan region, it has been found that lower mountains provide enough lift to break the cap and allow deep convection to break out (Medina et al. 2010). Previous studies of the storms in southeastern South America (Salio et al. 2007; Borque et al. 2010) have speculated that complex mesoscale flow patterns and frontal lifting are important in convective initiation and destabilization of the environment. Nevertheless, it is hard to ignore the robust statistics from Zipser et al. (2006) and Romatschke and Houze (2010) showing that the highest frequency of deep convective cores is found in the Sierra de Cordoba range and nearby Andean foothills. In addition, Borque et al. (2010) found an MCS genesis region directly over the Sierra de Cordoba Mountains. A high-resolution

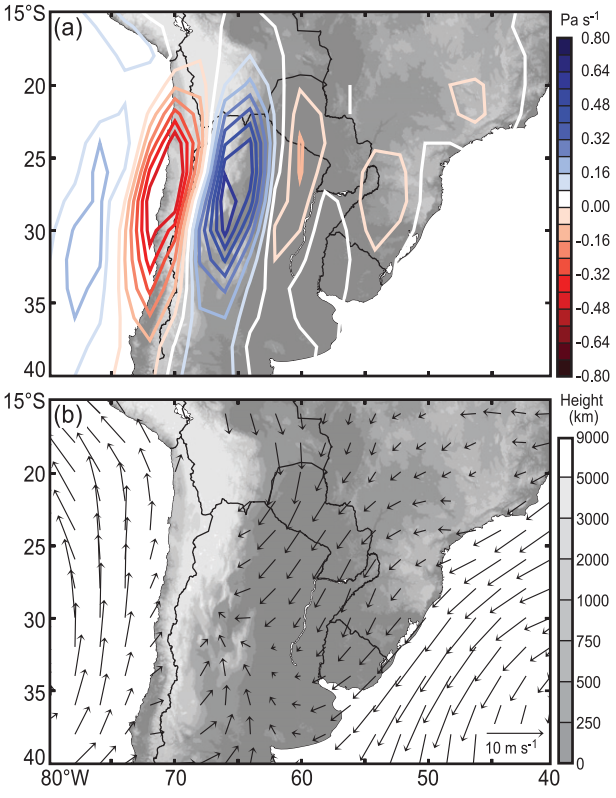

FIG. 8. Climatological composite maps for days on which the TRMM PR showed storms containing wide convective cores over the Sierra de Cordoba and La Plata North and South regions. (a) Omega or vertical motion (Pa s^{-1}) climatology contours at 700 hPa. Negative values (red contours) indicate upward motion and positive values (blue contours) indicate downward motion. (b) Composite wind vectors at 1000 hPa.

model study of severe zonda wind cases (foehn effect in South America) revealed that preceding frontal passages, zonda winds are associated with a vertical motion pattern consistent with Fig. 8a (Seluchi et al. 2003a). Air motions qualitatively similar to the zonda may occur to a lesser extent in many cases.

''Elevated convective initiation'' (Wilson and Roberts 2006; Marsham et al. 2011) is also not likely to be an alternative explanation for the deep convective triggering in southeastern South America as that mechanism involves air lying above a preexisting cold pool associated with a front or earlier MCS. The SALLJ flowing along the edge of the Andes traverses a path in which such low-level cold layers are generally not present. The unambiguous signature of orographic convective triggering centered on the Sierra de Cordoba Mountains (section 3b and Romatschke and Houze 2010) further indicates that it is the SALLJ encountering terrain features that is mostly responsible for the convective triggering in the western part of Argentina. Elevated convection may, on the other hand, occur above MCS cold pools or cold fronts farther to the east, over central Argentina. As also noted in section 3b and by Romatschke and Houze (2010), larger mesoscale systems with wide convective cores and broad stratiform regions occur frequently over that region. Analyzing satellite infrared imagery, Velasco and Fritsch (1987) and Laing and Fritsch (1997) also noted long-lived mesoscale systems moving eastward over central Argentina, and elevated initiation might be expected to contribute to the continued redevelopment in their eastward progression. Orographic triggering is clearly important, if not dominant, in southeastern South America, and deserves further investigation using a high-resolution model.

5. Case studies of storms with wide convective cores in the La Plata Basin

The analysis of TRMM data is limited to the statistics of snapshots in different storms, where they are randomly at different stages of development. As noted above, the statistics of the TRMM PR data summarized in Figs. 5 and 6 and the results of Romatschke and Houze (2010) suggest that the storms with wide convective cores represent a mature stage of storm development and that these storms are systematically orogenic, forming over the lower mountains to the east of the Andes and moving eastward across the plains toward the ocean. To determine if these statistical impressions are valid, we undertook case study examinations of some of the best-defined cases. Analyses of these cases can include other types of data, allowing for the TRMM data to be placed within the context of the life cycles of the storms. For the case study analyses, NCEP–NCAR reanalysis data were used due to the scarcity of surface and upper-air observations in southeastern South America. Storms with wide convective cores occur in connection with a low-level northerly jet (Fig. 4), which implies that they are more likely to contain tornadic convection. To prepare for an in-depth case study analysis, we conducted an informal perusal of the data for 50 cases containing the most intense deep convective cores, wide convective cores, and broad stratiform regions. The following two case studies exemplify the results of our case study analysis.

a. 26–27 December 2003

A wide convective core case of particular practical interest was detected by the TRMM PR at 1002 UTC on 27 December 2003. According to local media, this storm caused four fatalities, 90 injuries, 400 evacuees to flee the area, a strong tornado in Cordoba (eastern foothills

of the Sierra de Cordoba), hail, winds up to 35 m s^{-1}, very heavy rainfall rates, flooding, and power outages. With 326 lightning flashes and a convective rain percentage of 74%, this case falls within the midrange of wide convective cores in Figs. 3a and 3b.

The geosynchronous infrared satellite data show the temporal context of this case (Fig. 9). At 1745 UTC on 26 December 2003 (Fig. 9b), convective cells were triggered on the eastern side of the Sierra de Cordoba range. These cells were generated before the TRMM PR data captured this case as a wide convective core, which is consistent with the idea that the smaller mountains trigger deep convective cores, which organize into wide convective cores. The cold cloud top remained tied to the Sierra de Cordoba through about 1145 UTC the following day. Another interesting feature of this case is that its circular structure in the cloud-top temperature field could be classified as an MCC by the criteria of Maddox (1980) from 0845 to 1445 UTC. Velasco and Fritsch (1987) and Salio et al. (2007) have previously noted such systems in South America. The TRMM PR data add three-dimensional structural information to this prior research.

The 500-hPa geopotential height anomalies for the 27 December case study (Fig. 10a) show a low pressure anomaly (trough) directly over the southern Andes. Moderate northwesterly winds at 500 hPa flowed over the region of the storm. At the surface, a moderate low pressure anomaly was located east of the Andes (Fig. 10b). The surface map also shows a signature of the SALLJ located just east of the Andes. Figure 10b further shows that the Sierra de Cordoba range lies within a strong 1000–500-hPa thickness gradient, indicating that conditions in the region were baroclinic. Strong downslope flow off the Andes occurred directly to the west of the Sierra de Cordoba range. Warm air was present in most of southeastern South America (Fig. 10c) from two different sources: the Amazon basin via the low-level jet and the Atlantic Ocean. The warmest air was concentrated against the foothills of the Andes in the exact location of the storm. Figure 10d further shows that an extremely strong meridional gradient in the equivalent potential temperature was centered over the Sierra de Cordoba range. Large values of dewpoint depression are almost parallel to contours of equivalent potential temperature close to the Andes foothills, which are associated with dry air flowing off the mountains. Strong low-level convergence directly over the Sierra de Cordoba mountain range (Fig. 10c) was consistent with the triggering of cells directly over and to the east of this topographic feature. All of these observations together indicate that low-level orographic convergence, where the SALLJ encountered the Sierra de Cordoba terrain, was able to lift warm, moist air enough to break through the capping effect, which is likely due to leeside subsidence (Fig. 8) and, thus, allowed violent convection to occur and grow into the mesoscale system seen in Fig. 9.

The TRMM PR reflectivity data containing the wide convective core embedded in the storm were obtained at 1002 UTC 27 December 2003 and are overlaid on *GOES-12* infrared satellite brightness temperature data in Fig. 11a. This time was in the period when the satellite image properties qualified the storm as an MCC (Fig. 9). The wide convective core had a 40-dBZ contiguous echo exceeding 15 000 km^2 in area, in addition to a 16-km 40-dBZ echo height, which also qualified the storm for the deep convective core category. The radar echo had mesoscale organization with an east-southeast–west-northwest-oriented leading line of convection on its northern side and stratiform precipitation to the south of the line. Smaller, discrete lines of intense convection lay within the band; furthermore, these smaller elongated convective elements had a south-southeast–north-northwest orientation forming at an acute angle to the main line of convection. The horizontal radar echo structure is reminiscent of cases analyzed by Houze et al. (1990), who determined that the tendency for major rainstorms in Oklahoma was to have mesoscale radar echo structures with a leading-line/trailing-stratiform structure.

A vertical cross section of the TRMM PR data shows a deep convective core with very intense values of reflectivity and a region of stratiform precipitation (as indicated by the brightband) behind it (Fig. 11b). The convective core contained a 40-dBZ echo up to 12 km and had an overall echo top over 16 km. Also evident is an anvil-like structure to the right (ahead) of the convective cell, indicating strong upper-level outflow on the forward side of the storm. Because of the limited sensitivity of the TRMM PR (~17-dBZ minimum threshold), the full extent of this anvil structure cannot be seen. A sounding extracted from the NCEP–NCAR reanalysis fields in the inflow region of the storm (location indicated by the red dot in Fig. 11a) shows a stable layer near the surface, with a conditionally unstable layer from 850 to 600 hPa. Orographic lifting over the Sierra de Cordoba and/or cold-pool outflow from the developed storm must have removed this inversion in order for the air to have obtained the buoyancy to produce the deep convective core. Winds were veering (Fig. 11c, inset) with height, indicating warm-air advection. A low-level jet was present, with a counterclockwise hodograph favorable for tornadic storms [applying the results of Maddox et al. (1980) and Maddox (1976) in a Southern Hemisphere context]. A high value of convective available potential energy (CAPE) of 2747 J kg^{-1} and severe

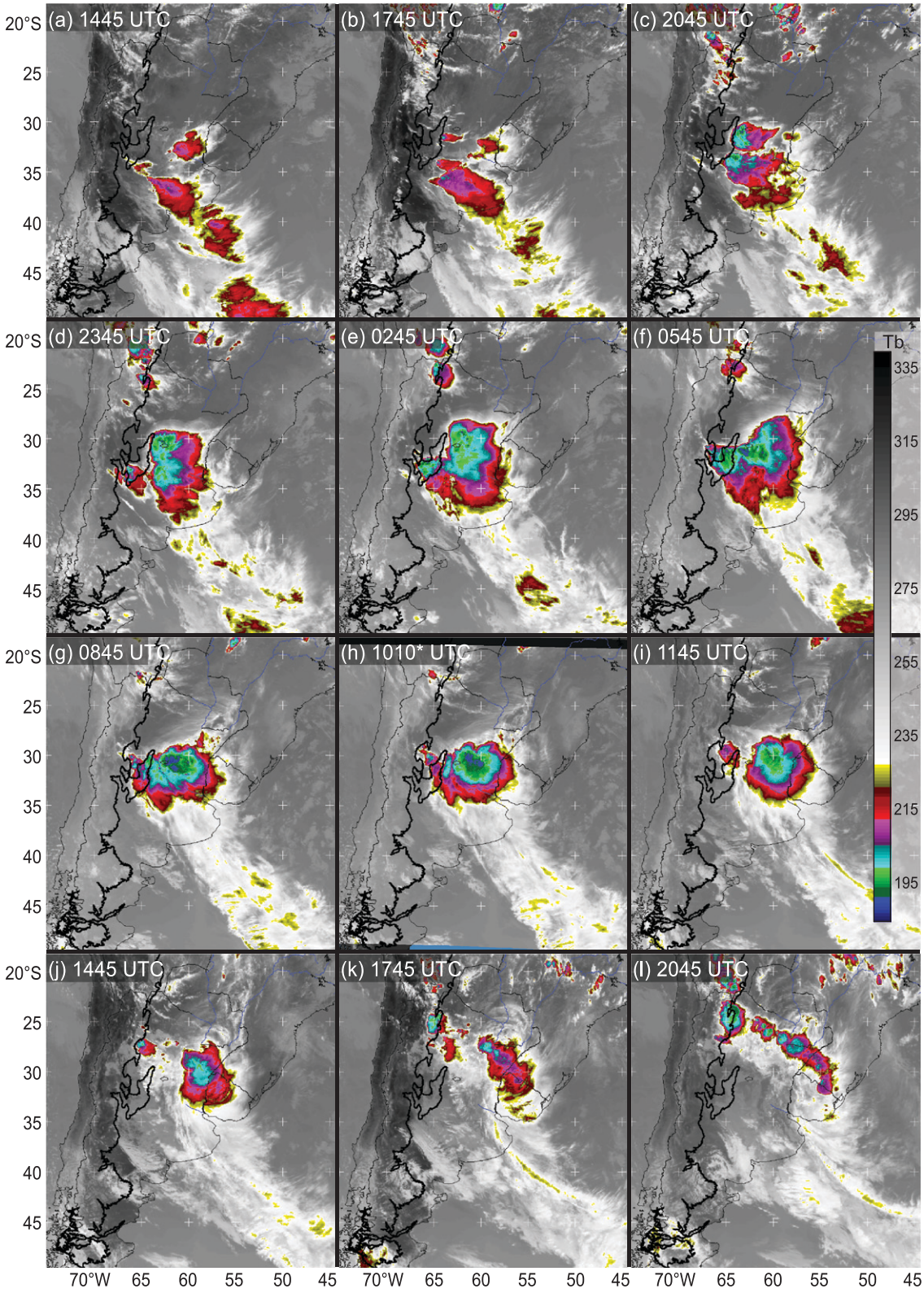

FIG. 9. Sequence of IR satellite images (K) showing storm triggering and evolution for the 26–27 Dec 2003 wide convective core. IR data are taken from *GOES-12*. The closest IR satellite image to the TRMM PR swath identified as a storm with a wide convective core is shown in (h), highlighted by the asterisk (*) symbol. The thick black contour outlines the 0.5-km topography.

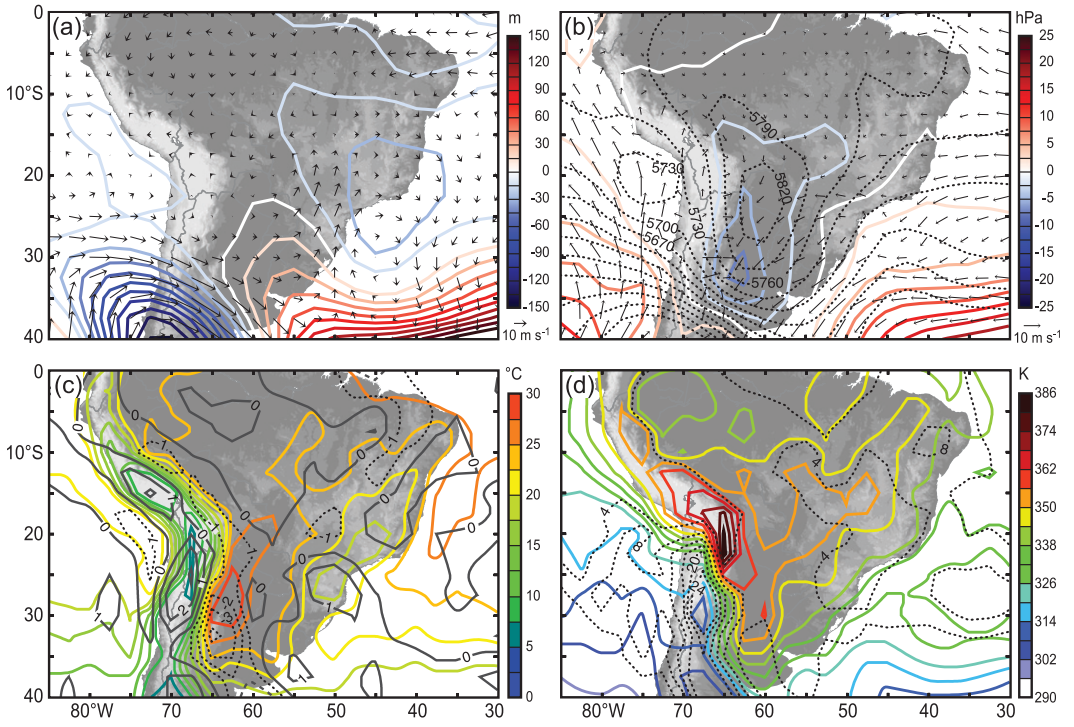

FIG. 10. Synoptic setting for the 27 Dec 2003 case that was identified as a storm with a wide convective core by the TRMM PR. Climatological conditions are defined as September–April (1948–2009). (a) Geopotential height anomalies and wind vectors at 500 hPa. The contours show the departure of the height (m) from the climatological 500-hPa surface. (b) Surface pressure anomalies, 1000–500-hPa thickness, and surface wind vectors. Colored contours show the departure (hPa) of the sea level pressure field from climatological conditions. Dotted contours show the 1000–500-hPa thickness (m) with greater thickness values indicating a warmer 1000–500-hPa layer. (c) Surface air temperature (°C) shown in colored contours and surface wind divergence. Dotted lines show negative values of divergence, or convergence of wind vectors. (d) Equivalent potential temperature (K) shown in color contours and dewpoint depressions at 925 hPa. Dotted lines indicate dewpoint depressions where higher values indicate drier air. Note that the topographic scale for (a)–(d) is the same as in Fig. 7.

lifted index and *K* index values were also consistent with the intensity of the convection and severe weather reports.

b. 12 November 2003

It is not uncommon for storms containing wide convective cores to cause severe damage, injury, and loss of life in the La Plata Basin region. Here, we present another example. In this case, a storm containing a wide convective core (according to local media) caused 14 fatalities, at least one strong tornado, winds in excess of 60 m s^{-1}, tennis-ball-sized hail, power outages, flooding, and intense rain rates. Of all the wide convective cores identified in 11 yr of TRMM data, the wide convective core in this storm was the largest, with a 40-dB*Z* contiguous echo covering about 38 000 km^2. The storm had 663 lightning flashes and a large convective rain percentage (94%). This case contrasts with the one from the previous section in that it occurred in conjunction with stronger baroclinic forcing. Romatschke and Houze (2010) have pointed out the tendency for storms with wide convective cores in South America to be associated with the passage of midlatitude baroclinic troughs. Our examination of approximately 50 of the largest wide convective core cases in all of South America indicates that 80% of them were associated with the passage of baroclinic troughs. The frontal forcing in the current case probably contributed to the excessive size of the system. According to Maddox (1983), both MCCs and tornadic storms often precede or accompany frontal passages.

The synoptic situation could be interpreted as the type described by Garreaud and Wallace (1998). They described a common synoptic situation in southeastern South America during the summer season, in which transient incursions of cold midlatitude air collide with warm, moist air over the continent, thus forming an ideal environment for deep convection in the Sierra de Cordoba and La Plata Basin South regions. The geopotential height anomalies at 500 hPa (Fig. 12a) show upper-level low pressure centered over the Andes

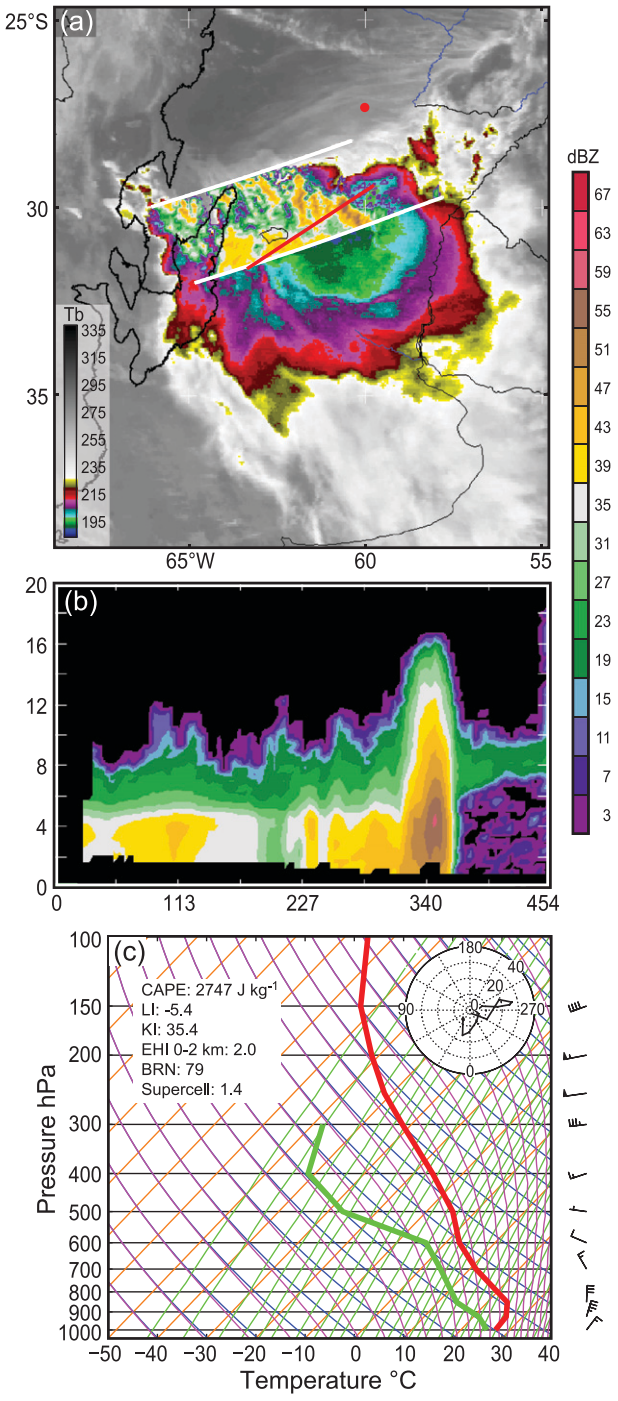

FIG. 11. Storm that was identified by the TRMM PR as containing a wide convective core at 1002 UTC 27 Dec 2003. (a) Reflectivity from the TRMM PR in dBZ at 4 km overlaid on the IR satellite brightness temperature (K). The white lines indicate the TRMM PR swath and the red line indicates the location of the vertical cross section. The thick black contour outlines the 0.5-km topography. (b) Vertical cross section taken along the red line in (a) of the TRMM PR data. (c) Sounding extracted from NCEP–NCAR reanalysis data at the location of the red dot in (a). The red line indicates the vertical temperature profile and the green line indicates the dewpoint temperature profile. Wind barbs are plotted to the right, corresponding to each vertical level and a hodograph is inset in the top-right corner. Various severe storm indices are visible in the top-left corner.

around 35°S. A strong surface low pressure anomaly was located east of the Andes with a center at about 32°S (Fig. 12b). The low anomaly in relation to the thickness field has a classic frontal structure. A strong SALLJ was feeding warm air directly into the frontal zone. Southerly winds behind the front were advecting colder air toward the rear of the storm. Strong downslope winds were occurring over the foothills of the Andes, adding to the convergence in the region.

A warm pocket of air was located over much of southeastern South America, extending from the Sierra de Cordoba range east to Uruguay and north to Paraguay (Fig. 12c). The SALLJ (seen in Fig. 12b) was advecting this warm air from the Amazon basin into the region of the storm. A large region of convergence occurred in the same area, with a strong maximum over the same region as the surface low pressure anomaly (Fig. 12c). A zonal gradient of equivalent potential temperature was located just east of the Sierra de Cordoba range (Fig. 12d), while relatively dry air from downslope flow off the Andes lay to the west and cold, dry air entered the region from the south. The dewpoint depression (dotted contours) field shows the contrasting humidity of the SALLJ air and the air behind the front (Fig. 12d).

The TRMM PR data show that the 12 November 2003 wide convective case was clearly line organized and large in horizontal extent in plan view (Fig. 13a). An infrared satellite loop from 10 through 13 November (not pictured) indicates that convective cells were triggered over or near the Sierra de Cordoba Mountains. Despite the fact that the TRMM PR swath truncated the radar echo, it is evident from this figure that the mature system had the structure of a classic leading-line/trailing-stratiform squall-line system (Houze et al. 1990). Its location along a frontal zone suggests that the mesoscale system was either forced or reinforced by frontogenetic processes after it was triggered. A vertical cross section running lengthwise along the convective line (Fig. 13b) shows that the very intense pockets of convection were typically confined to the lowest 4–6 km, which indicates that although this is a wide convective core of great horizontal extent, the heights of the 40-dBZ echoes were not generally extremely deep at this stage of the storm. A thermodynamic profile (Fig. 13c) extracted from the

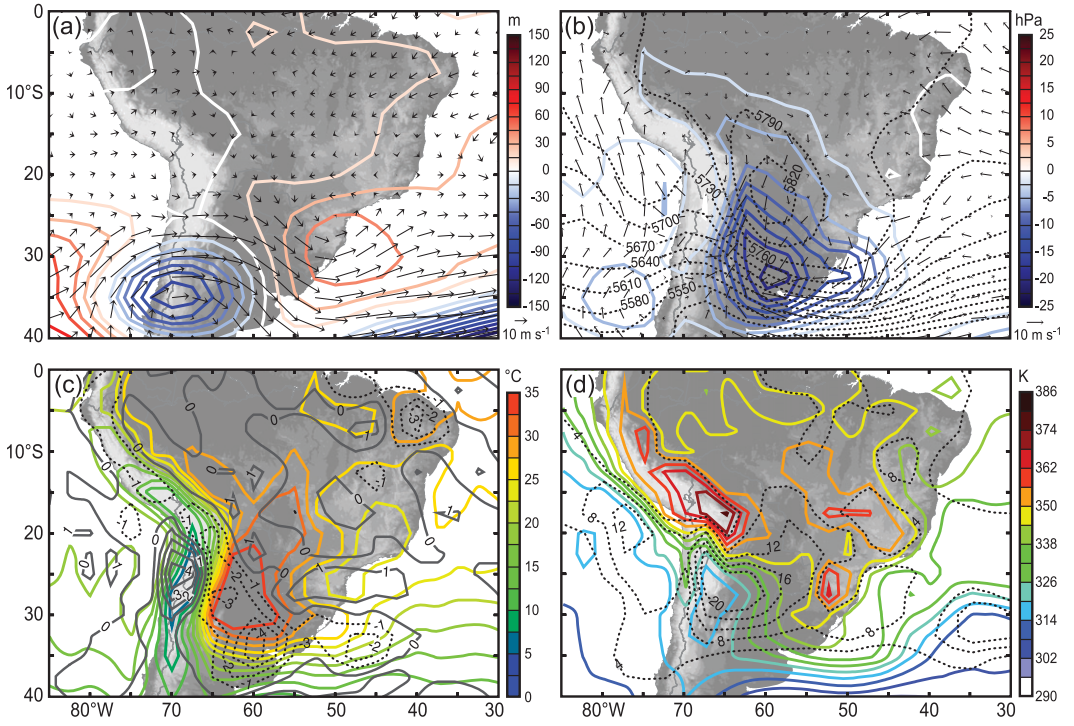

FIG. 12. As in Fig. 10, but for 12 Nov 2003.

NCEP–NCAR reanalysis data shows that the inflow region of the storm (location indicated by the red dot in Fig. 13a) had the characteristics of a severe storm sounding. The sounding shows a conditionally unstable layer from 925 to 300 hPa, with a very large value of CAPE (3168 J kg^{-1}), severe values for the lifted and *K* indices, and a strong energy–helicity index (EHI), indicating possible tornado formation. In addition, an inversion near the surface with drying above indicates that subsidence on the leeward side of the Andes was inhibiting the outbreak of convection until the air was lifted by either the Sierra de Cordoba range, the front, or the cold-pool outflow from the mesoscale convective system. Very strong wind shear with winds turning counterclockwise with height (veering) indicates strong warm advection combined with a low-level jet. The wind shear was generally consistent with that conducive to mesoscale line organization (Weisman and Klemp 1982; Rotunno et al. 1988; Houze et al. 1990).

6. Mesoscale storm organization

Previous studies of storms in subtropical South America have focused mainly on individual case studies, storm tracks, and synoptic-scale features (Seluchi et al. 2003b; Anabor et al. 2008; Garreaud and Wallace 1998). After our case study examination of approximately 50 storms containing the largest wide convective cores seen by the TRMM PR, it appeared that these wide convective cores tended to be located within larger contiguous radar echoes containing a line organization such as that seen in the two example case studies previously summarized. To test this impression, we carried out a systematic analysis of the morphology of the storms in the La Plata Basin and surrounding regions that contained wide convective cores. For this test, we employed a method similar to that used by Houze et al. (1990) to study heavy rainstorms in Oklahoma and by Schiesser et al. (1995) to analyze hailstorms in Switzerland. Applying their methodology to the TRMM PR database of storms with wide convective cores in South America, we have ranked TRMM-observed storms according to their similarity to the leading-line/trailing-stratiform schematic used by Houze et al. (1990).

The schematic is shown in Fig. 14, flipped vertically on the page to create what we have observed to be the Southern Hemisphere equivalent of the Oklahoma schematic. The shaded regions in Fig. 14 indicate increasing levels of reflectivity echo, which is measured by the TRMM PR. Seven out of 10 storm characteristics used by Houze et al. (1990) to characterize the storm structure relate directly to the leading convective line, and the more prominent of these are indicated in Fig. 14. The remaining three storm characteristics were used to classify the trailing-stratiform region. The 10 characteristics that they used are as follows:

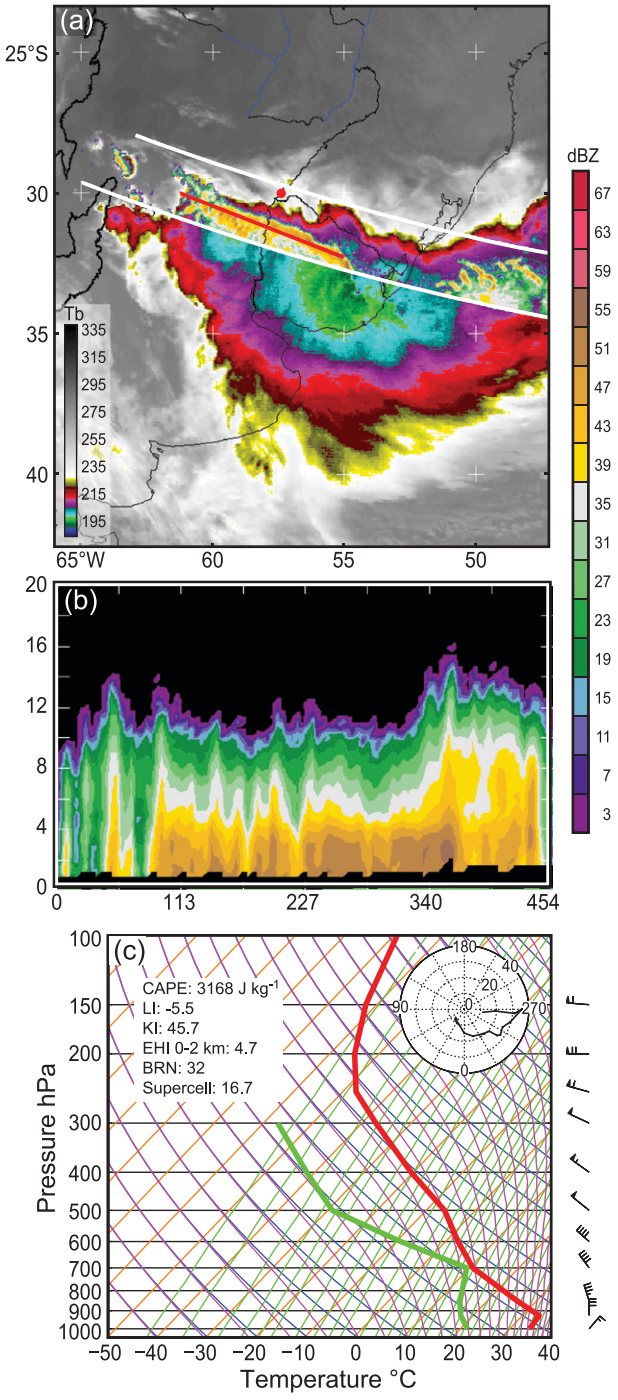

FIG. 13. As in Fig. 11, but for 12 Nov 2003.

1) The convective line should be arc shaped and convex toward the leading edge.
2) The line should be oriented in a northwest to southeast direction [changed for the Southern Hemisphere; Houze et al. (1990) used southwest to north-northeast].

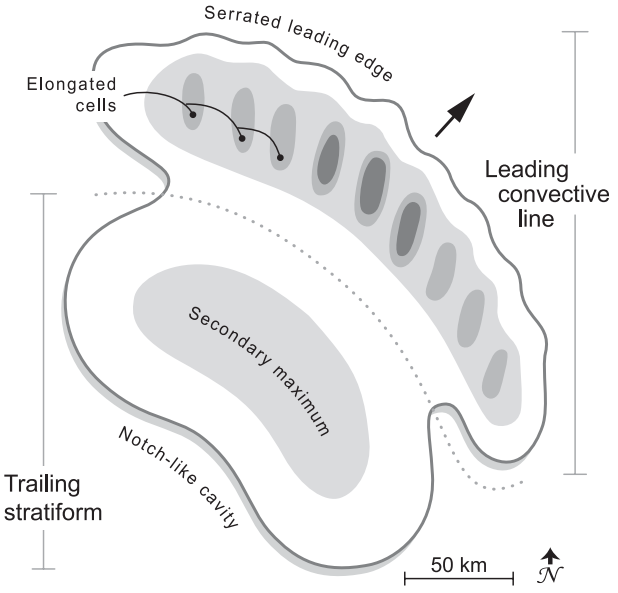

FIG. 14. Schematic of the leading-line/trailing-stratiform archetype described in Houze et al. (1990), but reoriented for study in the Southern Hemisphere. Increasing levels of shading indicate more intense radar reflectivity. As described in section 6, storms with wide convective cores were systematically compared to this idealized structure.

3) Line motion should be normal to the orientation of the line and must be >10 m s^{-1}. For this study, the relative line motion was estimated based on satellite data.
4) A solid leading line with intense convective cells should be connected by moderate reflectivity (see Fig. 14).
5) A strong reflectivity gradient must be present at the leading edge of the convective line.
6) As seen in Fig. 14, the leading edge of the convective line must be serrated or jagged, with protrusions at a wavelength of 5–10 km. This characteristic is now thought to be associated with roll vortices oriented parallel to the direction of the inflow to the mesoscale updraft maintaining the line; see Bryan et al. (2007) and further discussion in Houze (2004).
7) Cells within the convective line should be elongated with an orientation of 45°–90° to the leading line. This characteristic is indicated in Fig. 14 and is related to the serrated leading edge.
8) The trailing-stratiform region must be large in size and cover a region >10 000 km^2. The size was measured by the TRMM PR convective/stratiform echo separation algorithm.
9) As indicated in Fig. 14, a notchlike concavity should be present at the rear edge of the storm. This characteristic is associated with rear inflow at midlevels

TABLE 2. Summary of mesoscale organization based on the leading-line/trailing-stratiform archetype from Houze et al. (1990) shown in Fig. 14. Storms with wide convective cores were rated based on the 10 characteristics described in section 6. The *C* score is the classifiability of the storm. Percentages are based on the total number of storms analyzed in each study.

Degree of organization	Range of scores	Southeastern South America	Oklahoma (Houze et al. 1990)	Switzerland (Schiesser et al. 1995)
Strongly classifiable	$C > 5$	11 (20%)	14 (22.2%)	0 (0%)
Moderately classifiable	$0 \leq C \geq 5$	30 (54.5%)	18 (28.6%)	12 (21.4%)
Weakly classifiable	$C < 0$	7 (12.7%)	10 (15.9%)	18 (32.1%)
All classifiable systems	All *C*	48 (87.3%)	42 (66.7%)	30 (53.6%)
All unclassifiable systems	—	7 (12.7%)	21 (33.3%)	26 (46.4%)
Total No. of storms analyzed	—	55	63	56

as described by Smull and Houze (1985, 1987). They found that this air was generally dry and eroded stratiform echo in this region.

10) The stratiform region must contain a secondary maximum in echo intensity that is separated from the leading convective line by a region of less intense reflectivity.

Skamarock et al. (1994), Pandya and Durran (1996), and Pandya et al. (2000) have shown that the mesoscale organization prescribed by those 10 characteristics is reproduced in numerical models. They further showed that the tendency for some storms to have an ''asymmetric'' structure, with the trailing-stratiform region located on the poleward side of the system, was induced by the Coriolis force acting on the aging systems.

We followed exactly the methodology of Houze et al. (1990), which was to visually examine the radar echoes of each convective system for the presence or absence of the 10 characteristics related to the idealized schematic. We rated 55 of the most intense wide convective cores identified in 11 yr of TRMM PR data in South America. To reduce the uncertainty, this procedure was repeated three times, with both authors present and viewing the same data each time as well as checking and rechecking previous ratings. During one of the three rating procedures, all images were randomized and flipped vertically (resembling storms in the Northern Hemisphere) to prevent recognition of individual cases from previous analyses. For each of the 10 storm characteristics, the degree to which the TRMM PR data resembled the leading-line/trailing-stratiform model in Fig. 14 was determined by scoring 1 point if the feature or threshold was unambiguously present and −1 if it was definitely not present. In cases where a particular characteristic was to some degree present or absent, a score of 0.5 or −0.5 was assigned, respectively. If the particular characteristic was indeterminable from the available data, a score of 0 was given. Once all 10 characteristics were scored, the *C* or ''classifiability'' score was determined by taking the sum of the individual characteristic rankings. The *C* scores between 5 and 10 are considered to be ''strongly classifiable,'' scores between 0 and 5 are ''moderately classifiable,'' and scores between −10 and 0 are ''weakly classifiable'' storms. Storms with wide convective cores that did not exhibit any leading-line/trailing-stratiform signature at all were designated as ''unclassifiable'' storms.[2] We did not attempt to determine whether the storms had symmetric or asymmetric variations on the schematic structure in Fig. 14.

The results of the leading-line/trailing-stratiform study are summarized in Table 2. In general, the degree to which storms containing wide convective cores resemble the leading-line/trailing-stratiform archetype in southeastern South America is similar to the tendency of the Oklahoma storms studied by Houze et al. (1990) to exhibit this structure. The subdivision of the storms into strongly and weakly classifiable categories was in about the same proportion for the two regions. The storms in the La Plata Basin, east of the Andes, occur under similar conditions to the storms over the U.S. Great Plains, east of the Rocky Mountains (Carlson et al. 1983; Velasco and Fritsch 1987). Additionally, pronounced elongated cells have been observed in numerous storms with wide convective cores in southeastern South America and have also been documented in U.S. Great Plains squall-line systems (Ligda 1956; Houze et al. 1990; Bryan et al. 2007; Marsham et al. 2011). The storms in Switzerland studied by Schiesser et al. (1995) occur under rather different synoptic and topographic conditions, and they exhibited somewhat different characteristics, having no cases in the strongly classifiable category and increasing numbers of less organized systems.

Further comparison to Houze et al. (1990) is presented in Table 3, which shows the average number of severe storm reports per event with wide convective cores by degree of organization. The storm report

[2] A full, detailed table of every wide convective core that we examined is provided online (www.atmos.washington.edu/~kristen/research/paper/mesoscale_org.pdf).

TABLE 3. Average number of severe storm reports per storm with a wide convective core by degree of organization. Storm reports are derived from local media reports in South America and TRMM products. The criteria for each storm report category are described in Table 1.

Degree of organization	Lightning flashes	Fatalities	Hail	Tornado	Flooding	Heavy rain	Power outage	Strong winds	Evacuated	Total No. of storm reports
Strongly classifiable	354	1.3	1	0.4	0.7	1.7	0.8	1.9	77.3	6.7
Moderately classifiable	340	0.4	0.9	0.2	1	1.4	0.7	1.1	422.9	5.5
Weakly classifiable	360	0	0.2	0	0.7	0.3	0.2	0.2	300	1.8

categories of fatalities, hail, tornadoes, heavy/record rain, power outages, strong winds, and total storm reports show a notable preference for strongly classifiable storms. This result differs from that obtained by Houze et al. (1990); the low-*C* categories in Oklahoma storms contained more severe storm reports in the tornado, hail, strong winds, and heavy/record rain categories.

Lightning flashes, flooding reports, and the number of evacuated people per system are the only storm report categories that do not exhibit a preference for strongly classifiable systems. Lightning and flooding are about equally likely in any of the three storm classifications. All three classifications can produce large numbers of evacuees. The average number of evacuees can be strongly influenced by a single event and is subject to media errors. In contrast to the numbers in Table 3, the storms in Oklahoma with strongly classifiable line organization had the highest numbers of lightning reports, with decreasing numbers for less strongly classifiable storms (Table 6 in Houze et al. 1990). However, these numbers may not be strictly comparable since lightning flashes in the South American storms were measured by the TRMM satellite, whereas the lightning reports in the Oklahoma storms were based on visual observations. The more widespread precipitation conditions in strongly classifiable storms may have inhibited visual observations. A larger database of storm reports for South America is probably needed for conclusive comparisons to storms in the United States, as mentioned by Nascimento and Doswell (2005). Nonetheless, substantial differences between line-organized storms in Oklahoma and South America are suggested by Tables 2 and 3.

7. Conclusions

In South America, three distinct categories of storms have been identified from 11 yr of TRMM PR data as storms that contain radar echoes of extreme vertical or horizontal dimensions. Following Houze et al. (2007), Romatschke et al. (2010), and Romatschke and Houze (2010), these extreme echo structures are called deep convective cores, wide convective cores, and broad stratiform regions. The most frequent types of storms with these extreme echo forms are those containing wide convective cores. Storms containing wide convective cores produce some of the largest volumetric rain amounts. The bigger systems often qualify as MCCs in terms of the size and coldness of their cloud tops seen in infrared satellite imagery. Their rainfall is a relatively even mix of convective and stratiform components. TRMM measurements show that they exhibit frequent lightning flashes. Media reports show that they produce floods, tornadoes, and hail. They have societal impacts in the form of injuries, evacuations, and even fatalities.

The storms containing wide convective cores tend to be largest and most intense in the La Plata Basin and surrounding regions. Because of the importance of this category of storm, we have examined the storms in the La Plata Basin region that contained the 50 largest wide convective core echoes. These especially intense storms tend to occur when baroclinic troughs pass over the southern Andes. The large intense storms in the La Plata Basin region sometimes, but not always, occur in connection with cold fronts embedded in the baroclinic troughs. In either case, intense convection tends to be triggered at the eastern edge of the Andes. They have a strong tendency for their first cells to be generated over the foothills of the Andes or the Sierra de Cordoba range in Argentina. The latter is a favored location, as it lies directly in the path of the climatological SALLJ, which feeds warm, moist, low-level air southward along the edge of the Andes. After the convective cells are triggered over this terrain, they tend to first produce storms with deep convective cores, which are also favored in this region (Romatschke and Houze 2010). They grow into wider systems as the storms move to the east and over the La Plata Basin, where the storms containing wide convective cores are most frequent, and where the storms develop large stratiform regions along with the wide convective cores. Over time, they develop even larger stratiform regions as they continue eastward toward the Brazilian Highlands and Atlantic Ocean, where Romatschke and Houze (2010) found a maximum occurrence of storms with broad stratiform regions.

The large storms containing wide convective cores in the La Plata Basin region contain elements of both convective and stratiform precipitation (Fig. 3). Moreover, they frequently exhibit mesoscale organization, such that they are composed of a leading line of intense convective rain cells followed by a region of stratiform precipitation. The horizontal arrangement of convective and stratiform regions in a mesoscale convective system is an indicator of the internal organization of the system. Therefore, we subjected the storms that the TRMM PR data showed to contain wide convective cores to an analysis of the type carried out by Houze et al. (1990) for Oklahoma rainstorms and Schiesser et al. (1995) for Swiss hailstorms. This exercise revealed that the storms with wide convective cores over southeastern South America were generally similar in mesoscale organization to the Oklahoma rainstorms, but not similar to the Swiss storms. The idea that South American and U.S. mesoscale systems resemble each other has been circulating in the literature for around 30 yr. The present study confirms that notion.

The strongly and moderately classifiable forms of leading-line/trailing-stratiform organization were the dominant organization types in both the southeastern South American storms and the Oklahoma storms, while a relatively small percentage of storms showed no inclination toward this form of organization. The Swiss storms, on the other hand, are much less likely to have a leading-line/trailing-stratiform mesoscale structure. The tendency for the South American storms to be more like the Oklahoma storms is understandable in that both storm regions have mountains lying to the west that channel low-level moist flow poleward, and both regions are located near the equatorward extremity of baroclinic influence, allowing troughs and fronts to often affect the storm organization. In the case of the Oklahoma storms, orographic triggering is not evidently the primary triggering mechanism in the region; the storms tend to be triggered by some other form of low-level convergence, usually a front or dryline. Well-known exceptions, of course, occur. Topographic features occasionally influence the triggering storms in the central United States (the Palmer Divide in Colorado or the aforementioned Cap Rock escarpment in northwestern Texas). However, close examination of the results of Zipser et al. (2006) reveals that the locations of the deepest convection over the United States do not climatologically cluster around any particular local topographic feature as it does in other regions such as southeastern South America or near the Himalayas (Romatschke et al. 2010; Romatschke and Houze 2010). This observation combined with previous studies suggests that orographic triggering plays a substantially larger role in southeastern South America than in the United States.

One notable difference between the storms in southeastern South America and those over the U.S. Great Plains is that the most mesoscale-organized South American storms produce more hail and tornadoes. We cannot say why this difference exists, but the wind shear profile in the air feeding the South American mesoscale leading-line/trailing-stratiform storms with wide convective cores tended to have counterclockwise shear of the SALLJ lower-level winds, which would favor the development of supercell hailstorms and tornadoes within the leading line of convection.

A further comparison of the South American storms containing wide convective cores can be made to storms containing wide convective cores in the western Himalayan region of Pakistan and northwest India. Moist flow from the Arabian Sea feeding the Himalayan systems is overridden by westerlies coming over the mountains to the west, as in the U.S. Great Plains and in southeastern South America. In the Himalayan case, baroclinic forcing plays little if any role, and the triggering of the intense convection occurs when the moist flow encounters lower mountains in front of the main Himalayan range (Houze et al. 2007; Medina et al. 2010). The South American and Himalayan storms are thus both primarily triggered by orographic forcing, which does not seem to be the primary triggering mechanism over the U.S. Great Plains. The South American and Oklahoma storms are affected by baroclinic forcing, which is absent in the Himalayan storms. Thus, extreme convection in all three regions east of major mountain ranges occurs with different combinations of determining factors. This study leads about as far as one can go with existing data alone in determining the nature of extreme convection in South America. To advance our understanding of these storms requires modeling. Studies such as Skamarock et al. (1994) have examined the Oklahoma type of storms via modeling and led to an explanation of the leading-line/trailing-stratiform structure of those storms. Medina et al. (2010) successfully improved our understanding of Himalayan storms via modeling. Following this path, we are presently undertaking a study using a high-resolution cloud-resolving model to study the storms with wide convective cores in southeastern South America. This work will be reported on in a forthcoming paper.

Acknowledgments. We acknowledge Stacy Brodzik and Ulrike Romatschke for assistance in processing the data used in this study. Socorro Medina provided tools for data analysis. Beth Tully processed the graphics, and Anthony Didlake commented on the manuscript.

The authors thank Dr. Ed Zipser and an anonymous reviewer for their comments and suggestions, which have greatly improved this manuscript. NCEP–NCAR and Twentieth Century reanalysis data were downloaded online (http://www.cdc.noaa.gov/). Support for the Twentieth Century Reanalysis Project dataset is provided by the U.S. Department of Energy/Office of Science's Innovative and Novel Computational Impact on Theory and Experiment (DOE INCITE) program, and the Office of Biological and Environmental Research (BER), and by the National Oceanic and Atmospheric Administration Climate Program Office. This research was sponsored by National Aeronautics and Space Administration Grant NNX10AH70G, National Science Foundation Grant ATM-0820586, and an American Meteorological Society Industry/Government Graduate Fellowship.

REFERENCES

Altinger de Schwarzkopf, M. L., and L. C. Russo, 1982: Severe storms and tornadoes in Argentina. Preprints, *12th Conf. on Severe Local Storms,* San Antonio, TX, Amer. Meteor. Soc., 59–62.

Anabor, V., D. J. Stensrud, and O. L. L. de Moraes, 2008: Serial upstream-propagating mesoscale convective system events over southeastern South America. *Mon. Wea. Rev.,* **136,** 3087–3105.

Awaka, J., T. Iguchi, H. Kumagai, and K. Okamoto, 1997: Rain type classification algorithm for TRMM Precipitation Radar. *Proc. 1997 Int. Geoscience and Remote Sensing Symp. (IGARSS '97)—Remote Sensing: A Scientific Vision for Sustainable Development,* Vol. 4, Singapore, IEEE, 1633–1635.

Borque, P., P. Salio, M. Nicolini, and Y. G. Skabar, 2010: Environment associated with deep moist convection under SALLJ conditions: A case study. *Wea. Forecasting,* **25,** 970–984.

Brooks, H. E., J. W. Lee, and J. P. Craven, 2003: The spatial distribution of severe thunderstorm and tornado environments from global reanalysis data. *Atmos. Res.,* **67-68,** 73–94.

Bryan, G. H., R. Rotunno, and J. M. Fritsch, 2007: Roll circulations in the convective region of a simulated squall line. *J. Atmos. Sci.,* **64,** 1249–1266.

Carlson, T. N., S. G. Benjamin, G. S. Forbes, and Y.-F. Li, 1983: Elevated mixed layers in the regional severe storm environment: Conceptual model and case studies. *Mon. Wea. Rev.,* **111,** 1453–1474.

Cecil, D. J., 2009: Passive microwave brightness temperatures as proxies for hailstorms. *J. Appl. Meteor. Climatol.,* **48,** 1281–1286.

——, 2011: Relating passive 37-GHz scattering to radar profiles in strong convection. *J. Appl. Meteor. Climatol.,* **50,** 233–240.

Compo, G. P., and Coauthors, 2009: The Twentieth Century Reanalysis Project. *Quart. J. Roy. Meteor. Soc.,* **137,** 1–28, doi:10.1002/qj.776.

Durkee, J. D., T. L. Mote, and J. M. Shepherd, 2009: The contribution of mesoscale convective complexes into rainfall across subtropical South America. *J. Climate,* **22,** 4590–4605.

Garreaud, R. D., and J. M. Wallace, 1998: Summertime incursions of midlatitude air into subtropical and tropical South America. *Mon. Wea. Rev.,* **126,** 2713–2733.

Houze, R. A., Jr., 2004: Mesoscale convective systems. *Rev. Geophys.,* **42,** RG4003, doi:10.1029/2004RG000150.

——, B. F. Smull, and P. Dodge, 1990: Mesoscale organization of springtime rainstorms in Oklahoma. *Mon. Wea. Rev.,* **118,** 613–654.

——, D. C. Wilton, and B. F. Smull, 2007: Monsoon convection in the Himalayan region as seen by the TRMM Precipitation Radar. *Quart. J. Roy. Meteor. Soc.,* **133,** 1389–1411.

Iguchi, T., T. Kozu, R. Meneghini, J. Awaka, and K. Okamoto, 2000a: Rain-profiling algorithm for the TRMM Precipitation Radar. *J. Appl. Meteor.,* **39,** 2038–2052.

——, R. Meneghini, J. Awaka, T. Kozu, and K. Okamoto, 2000b: Rain-profiling algorithm for TRMM Precipitation Radar data. *Adv. Space Res.,* **25,** 973–976.

Kalnay, E., and Coauthors, 1996: The NCEP/NCAR 40-Year Reanalysis Project. *Bull. Amer. Meteor. Soc.,* **77,** 437–471.

Laing, A. G., and J. M. Fritsch, 1997: The global population of mesoscale convective complexes. *Quart. J. Roy. Meteor. Soc.,* **123,** 389–405.

Liebmann, B., G. N. Kiladis, J. A. Marengo, T. Ambrizzi, and J. D. Glick, 1999: Submontly convective variability over South America and the South Atlantic convergence zone. *J. Climate,* **12,** 1877–1891.

Ligda, M. G. H., 1956: The radar observations of mature prefrontal squall lines in the midwestern United States. Summary, *Lectures Held during the VIth Congress of OSTIV,* St. Yan, France, Organisation Scientifique et Technique du Vol à Voile, 3 pp.

Maddox, R. A., 1976: An evaluation of tornado proximity wind and stability data. *Mon. Wea. Rev.,* **104,** 133–142.

——, 1980: Mesoscale convective complexes. *Bull. Amer. Meteor. Soc.,* **61,** 1374–1387.

——, 1983: Large-scale meteorological conditions associated with midlatitude, mesoscale convective complexes. *Mon. Wea. Rev.,* **111,** 1475–1493.

——, L. R. Hoxit, and C. F. Chappell, 1980: A study of tornadic thunderstorm interactions with thermal boundaries. *Mon. Wea. Rev.,* **108,** 322–336.

Marengo, J. A., W. R. Soares, C. Saulo, and M. Nicolini, 2004: Climatology of the low-level jet east of the Andes as derived from the NCEP–NCAR reanalyses: Characteristics and temporal variability. *J. Climate,* **17,** 2261–2280.

Marsham, J. H., S. B. Trier, T. M. Weckwerth, and J. W. Wilson, 2011: Observations of elevated convection initiation leading to a surface-based squall line during 13 June IHOP_2002. *Mon. Wea. Rev.,* **139,** 247–271.

Medina, S., R. A. Houze Jr., A. Kumar, and D. Niyogi, 2010: Summer monsoon convection in the Himalayan region: Terrain and land cover effects. *Quart. J. Roy. Meteor. Soc.,* **136,** 593–616.

Nascimento, E. L., and C. A. Doswell III, 2005: The need for improved documentation of severe thunderstorms and tornadoes in South America. Preprints, *Symp. on the Challenges of Severe Convective Storms,* Atlanta, GA, Amer. Meteor. Soc., P1.18. [Available online at http://ams.confex.com/ams/techprogram/paper_102247.htm.]

——, and I. P. V. O. Marcelino, 2005: Preliminary analysis of the 3 January 2005 tornadoes in Criciuma/SC (in Portuguese). *Bull. Braz. Meteor. Soc.,* **29,** 33–44.

Nogués-Paegle, J., and K. C. Mo, 1997: Alternating wet and dry conditions over South America during summer. *Mon. Wea. Rev.,* **125,** 279–291.

Pandya, R. E., and D. R. Durran, 1996: The influence of convectively generated thermal forcing on the mesoscale circulation around squall lines. *J. Atmos. Sci.,* **53,** 2924–2951.

——, ——, and M. L. Weisman, 2000: The influence of convective thermal forcing on the three-dimensional circulation around squall lines. *J. Atmos. Sci.,* **57,** 29–45.

Romatschke, U., and R. A. Houze Jr., 2010: Extreme summer convection in South America. *J. Climate,* **23,** 3761–3791.

——, S. Medina, and R. A. Houze Jr., 2010: Regional, seasonal, and diurnal variations of extreme convection in the South Asian region. *J. Climate,* **23,** 419–439.

Rotunno, R., J. B. Klemp, and M. L. Weisman, 1988: A theory for strong, long-lived squall lines. *J. Atmos. Sci.,* **45,** 463–485.

Salio, P., M. Nicolini, and E. J. Zipser, 2007: Mesoscale convective systems over southeastern South America and their relationship with the South American low-level jet. *Mon. Wea. Rev.,* **135,** 1290–1309.

Saulo, A. C., M. Nicolini, and S. C. Chou, 2000: Model characterization of the South American low-level flow during the 1997–1998 spring–summer season. *Climate Dyn.,* **16,** 867–881.

Sawyer, J. S., 1947: The structure of the intertropical front over NW India during the SW monsoon. *Quart. J. Roy. Meteor. Soc.,* **73,** 346–369.

Schiesser, H.-H., R. A. Houze Jr., and H. Huntrieser, 1995: The mesoscale structure of severe precipitation systems in Switzerland. *Mon. Wea. Rev.,* **123,** 2070–2097.

Seluchi, M. E., F. A. Norte, P. Satyamurty, and S. C. Chou, 2003a: Analysis of three situations of the foehn effect over the Andes (zonda wind) using the Eta–CPTEC regional model. *Wea. Forecasting,* **18,** 481–501.

——, A. C. Saulo, M. Nicolini, and P. Satyamurty, 2003b: The northwestern Argentinean low: A study of two typical events. *Mon. Wea. Rev.,* **131,** 2361–2378.

Skamarock, W. C., M. L. Weisman, and J. B. Klemp, 1994: Three-dimensional evolution of simulated long-lived squall lines. *J. Atmos. Sci.,* **51,** 2563–2584.

Smull, B. F., and R. A. Houze Jr., 1985: A midlatitude squall line with a trailing region of stratiform rain: Radar and satellite observations. *Mon. Wea. Rev.,* **113,** 117–133.

——, and ——, 1987: Rear inflow in squall lines with trailing-stratiform precipitation. *Mon. Wea. Rev.,* **115,** 2869–2889.

Tripoli, G. J., and W. R. Cotton, 1989: Numerical study of an observed orogenic mesoscale convective system. Part I: Simulated genesis and comparisons with observations. *Mon. Wea. Rev.,* **117,** 273–304.

Velasco, I., and J. M. Fritsch, 1987: Mesoscale convective complexes in the Americas. *J. Geophys. Res.,* **92,** 9591–9613.

Vera, C., and Coauthors, 2006: The South American Low-Level Jet Experiment. *Bull. Amer. Meteor. Soc.,* **87,** 63–77.

Weisman, M. L., and J. B. Klemp, 1982: The dependence of numerically simulated convective storms on vertical wind shear and buoyancy. *Mon. Wea. Rev.,* **110,** 504–520.

Wilson, J. W., and R. D. Roberts, 2006: Summary of convective storm initiation and evolution during IHOP: Observational and modeling perspective. *Mon. Wea. Rev.,* **134,** 23–47.

Zipser, E. J., D. J. Cecil, C. Liu, S. W. Nesbitt, and D. P. Yorty, 2006: Where are the most intense thunderstorms on earth? *Bull. Amer. Meteor. Soc.,* **87,** 1057–1071.